HHS Public Access

Author manuscript

J Immunol. Author manuscript; available in PMC 2017 August 15.

Published in final edited form as:

J Immunol. 2016 August 15; 197(4): 1408–1414. doi:10.4049/jimmunol.1600463.

Biophysical and biochemical characterization of avian secretory component provides structural insights into the evolution of the polymeric Ig receptor

Beth M. Stadtmueller[*], **Zhongyu Yang**[†,§], **Kathryn E. Huey-Tubman**[*], **Helena Roberts-Mataric**[*,‡], **Wayne L. Hubbell**[†], and **Pamela J. Bjorkman**[*]

[*]Division of Biology and Biological Engineering, California Institute of Technology, Pasadena, CA 91125 USA

[†]Jules Stein Eye Institute and Department of Chemistry and Biochemistry, University of California, Los Angeles, CA 90095 USA

[‡]South Pasadena High School, South Pasadena, CA 91030 USA

Abstract

The polymeric immunoglobulin receptor (pIgR) transports polymeric antibodies across epithelia to the mucosa, where proteolytic cleavage releases the ectodomain (secretory component; SC) as an integral component of secretory antibodies, or as an unliganded protein that can mediate interactions with bacteria. SC is conserved among vertebrates, but domain organization is variable: mammalian SC has five domains (D1-D5), whereas avian, amphibian and reptilian SC lack the D2 domain, and fish SC lacks domains D2-D4. Here we used double electron-electron resonance spectroscopy and surface plasmon resonance binding studies to characterize the structure, dynamics and ligand binding properties of avian SC, avian SC domain variants, and a human SC variant lacking the D2 domain. These experiments demonstrated that unlike human SC, which adopts a compact or "closed" domain arrangement, unliganded avian SC is flexible and exists in both closed and open states, suggesting that the mammalian SC D2 domain stabilizes the closed conformation observed for human SC D1-D5. Experiments also demonstrated that avian and mammalian pIgR share related, but distinct, mechanisms of ligand binding. Together, our data reveal differences in the molecular recognition mechanisms associated with evolutionary changes in the pIgR protein.

INTRODUCTION

Throughout vertebrate evolution, selective pressure to provide adaptive and innate immune responses in glandular and epithelial mucosa has resulted in the coevolution of secretory antibodies and the polymeric immunoglobulin receptor (pIgR) (1). The pIgR is synthesized as a transmembrane protein (2) that selectively transports polymeric antibodies (pIg) from the basolateral side of epithelial cells to the apical surface and releases them into the

Address correspondence and reprint requests to Pamela J. Bjorkman; Division of Biology and Biological Engineering, California Institute of Technology, Pasadena, CA 91125 USA. bjorkman@caltech.edu.

[§]Present address: Department of Chemistry and Biochemistry, North Dakota State University, Fargo, ND 50108 USA

mucosa, where the pIgR ectodomain, termed secretory component (SC), remains bound to the antibody (3). SC serves to shield secretory antibodies from proteolysis (4) and mediates interactions with host and bacterial factors (3). Together, these molecules protect vertebrates from the external environment, excluding pathogenic and toxic agents while also promoting host-bacterial mutualism with commensal agents (3). The pIgR is the earliest recognizable antibody Fc receptor, and along with its polymeric Immunoglobulin (pIg) ligands, is conserved from teleost (bony) fish to mammals (5). The pIgR has an extracellular region composed of tandem immunoglobulin-like (Ig-like) domains, a transmembrane region and a cytoplasmic tail (6); however, the domain organization of the extracellular region (hereafter referred to as secretory component; SC) is divergent among species (5,7) (Fig. 1A). Fish SC comprises two Ig-like domains (D1-D2) and associates with polymeric versions of IgM and IgT/IgZ, a teleost Ig specialized in mucosal immunity (8,9). In amphibians, the pIgR ectodomain contains four Ig-like domains (D1-D4) that bind polymeric forms of IgM and IgX, an amphibian mucosal antibody (10). Similar to amphibians, avian and reptilian pIgR also contain four extracellular domains, but bind to polymeric forms of IgM and IgA (pIgA), which assemble together with a protein called joining (J) chain (5,7,11). Mammalian SC also bind pIgs, typically dimeric IgA (dIgA) and pentameric IgM (pIgM), however a gene duplication event added a domain immediately following D1, enlarging mammalian SC to five Ig-like domains (D1-D5) (5,6). Phylogenic sequence analysis suggests that fish D1-D2 are homologous to mammalian D1 and D5, while avian D1-D2-D3-D4 are homologous to mammalian D1-D3-D4-D5 (8,12–14).

Although mammalian pIgR, pIgA, pIgM have been studied extensively, orthologous proteins in lower vertebrates are poorly characterized, limiting our understanding of how the mucosal immune system has adapted to meet species-specific requirements. We recently reported the crystal structures of human SC (hSC) and teleost fish SC (tSC), which revealed hSC D1-D5 in a compact triangular conformation and tSC D1-D2 in an elongated conformation (15). We have now evaluated avian SC D1-D4 structure, dynamics and ligand binding mechanisms using double electron-electron resonance spectroscopy (DEER) and surface plasmon resonance (SPR). Our results demonstrated that avian SC is highly dynamic, suggested that the addition of the D2 domain in mammals stabilized the compact triangular SC domain arrangement, and showed that avian and mammalian SC share related but distinct mechanisms of ligand binding. Together with previous results (15), these data allow us to correlate divergent SC conformational states and domain contributions to ligand binding with representative SC from each major branch in adaptive immune evolution.

MATERIALS AND METHODS

Construct design

A gene fragment (GenBank: NM_001044644) encoding the *Gallus gallus* pIgR signal peptide and ectodomain residues 1–444 (mature sequence numbering) as well as a C-terminal hexahistidine affinity tag was synthesized (Integrated DNA Technologies) and cloned into the pTT5 expression vector (NRC Biotechnology Research Institute) with a 5′ Kozak sequence. This construct was modified using site-directed mutagenesis to create *Gallus gallus* SC (ggSC) domain variants, chimeric SC, and mutants used for spin labeling.

The previously-described expression construct encoding hSC residues 1–549 (15) was modified using site-directed mutagenesis to create mutant hSC D1-D3-D4-D5 used for spin-labeling.

Protein preparation

All SC proteins were expressed using methods analogous to those published for hSC (15). Briefly, proteins were expressed in transiently-transfected HEK293-6E cells (NRC Biotechnology Research Institute) and purified using HisTrap and Superdex 200 chromatography (GE Healthcare). Proteins were maintained in TBS buffer (20 mM Tris-HCl, pH 7.4, 150 mM NaCl), which was supplemented with 250 mM imidazole for HisTrap elution. Human dIgA (provided by J. Vaerman; Catholic University of Louvain, Brussels, Belgium) and pIgM (Sigma-Aldrich) used for binding studies was purified using Superose 6 chromotography (GE Healthcare) as previously described (15).

ggSC molecular weight determination

To determine an absolute molecular weight, ggSC was evaluated using size exclusion chromatography (SEC) with in-line multi-angle light scattering (MALS) (16). Briefly, purified ggSC concentrated to 2.5 mg/ml in TBS buffer was evaluated using a Superdex 200 10/300 column (GE Healthcare) connected to a Dawn HELEOS II, DynaPro Nanostar, and Optilab t-rEX (Wyatt Technology, Santa Barbara, CA, USA). Multi-angle light scattering and refractive index data were collected at 25°C at a flow rate of 0.5 ml/min at 25 °C and analyzed using ASTRA 6 (Wyatt Technology). Data were exported and re-plotted for figures using Prism (GraphPad Software).

Nitroxide spin-labeling

SEC-purified, cysteine-substitution variants of ggSC and hSC (ggSC E352C/S387C, V76C/E352C, V76C/S387C, and hSC D1-D3-D4-D5 T67C/Q491C; all including C468A and C502A substitutions) were labeled with HO-225 reagent (2,2,5,5-tetramethyl-pyrroline-1-oxyl methanethiosulfonate), which generates the R1 side chain, as previously described for hSC variants (15). A protein filtration step, using a 0.2μm spin filter (Millipore), was added after initial exposure to HO-225 and prior to overnight incubation. The HO-225 reagent was the generous gift of Kalman Hideg (University of Pecs, Hungary).

DEER spectroscopy

Variants of ggSC and hSC proteins labeled with the R1 spin label were exchanged into TBS buffer containing 75% D_20 (Sigma-Aldrich; St. Louis, MO) and 20% (v/v) d-8 glycerol (Sigma-Aldrich). The final sample concentration ranged from 100–250μM. Samples of 15–20μl were loaded into glass capillaries (1.4 i.d. 1.7 o.d.; VitroCom Inc., NJ) and flash-frozen in liquid nitrogen. Similar to previously published methods (15), the Bruker ELEXSYS 580 system, operated at Q-band equipped with a cryogen-temperature controlling system, was used to perform four-pulse DEER data acquisition at 80K. A standard four-pulse DEER sequence $[(\pi/2)_{\nu o} - \tau_1 - (\pi)_{\nu o} - T - (\pi)_{\nu p} - \tau_2 - (\pi)_{\nu o} - \tau_1 - \text{echo}]$ was employed where ν_o and ν_p are the observed and the pump frequencies, respectively. A 36ns π– pump pulse was applied at a frequency corresponding to the maximum of the absorption spectrum of the

nitroxide, and the observer π/2 (16ns) and π (32ns) pulses were positioned 50 MHz (17.8 Gauss) upfield at the maximum of the center-field absorption line. The delay time τ1 was 200ns; τ2 varied from 3.0–6.0μs depending on the sample. The step size in all measurements was 16ns. Due to the use of the deuterated buffer, electron spin echo envelope modulation resulting from the interaction of nitroxide electron spin and the deuterium nuclei was averaged by adding traces at 8 different τ1 values, starting at 200ns and incrementing by 16ns. Distance distributions were obtained from the raw dipolar evolution data using the program LongDistance available at: http://www.biochemistry.ucla.edu/biochem/Faculty/Hubbell/. The upper limit of reliable distance (r) and width determination (σ) for each mutant in nanometers was calculated according to (17,18) as described in a previous publication (15).

Surface plasmon resonance

Surface plasmon resonance (SPR) binding studies were performed on a Biacore T200 instrument (GE Healthcare) using previously-reported methods (15). Briefly, human dIgA or pIgM was immobilized on three of four flow cells of CM5 biosensor chips (GE Healthcare) using primary amine coupling (Biacore manual). Ligand densities were 137, 483, and 790 resonance units (RUs) for the dIgA surfaces, and 517, 1779, and 3076 RUs for pIgM surfaces. The remaining flow cell was mock-coupled and used as a reference surface. The binding of all analytes was tested using a 2-fold dilution series in HBS-EP+ buffer (10mM HEPES pH 7.4, 150mM NaCl, 3 mM EDTA, 0.05% (v/v) P20). The highest concentration used for each analyte is provided in the figure legends. Data were collected at 25°C, and 2.5M $MgCl_2$ was used to regenerate all surfaces. Data were visualized and processed using T200 Evaluation software (GE Heathcare) and exported and re-plotted using Prism (GraphPad Software). Binding response data obtained for 32nM protein samples were normalized to the maximum binding response of each dataset.

Sequence alignments and SC modeling

IgA Sequence alignments utilized the constant heavy chain regions from *Gallus gallus* IgA (NCBI accession number: AAB22614.2), human IgA1 (NCBI accession number: AAC82528.1) and human IgA2 (NCBI accession number: AAB59396.1) http://www.ncbi.nlm.nih.gov/genbank. Sequence alignments of ggSC and hSC utilized the sequences from related expression constructs (this work and (15)). Alignments and figures were completed using Clustal Omega (19) and Espript 3 (20–22). The 10 N-terminal residues of mature ggSC (AKSRYPPKTS), which are not homologous to hSC and are predicted to be unstructured, were eliminated for clarity. Modeling of a D1-D3-D4-D5 structure was completed by removing residues 111–225 from the hSC crystal structure (pdb code: 5D4K) and then manually rebuilding a linker in Coot (23). The modeled linker sequence, QGPGLLNDA, comprises the human sequence followed by an Ala to create a linker the same length as the ggSC D1-D2 linker. The associated figure was made using the Pymol Molecular Graphics System (Schrodinger LLC).

RESULTS

Purification of avian SC

Avian SC protein was identified *in vivo* (24) and the gene encoding avian pIgR has been characterized (12), yet to the best of our knowledge an avian SC protein had not purified or biochemically characterized. To accomplish this, we synthesized a gene fragment encoding the chicken (*Gallus gallus*) pIgR ectodomain and created a mammalian expression vector encoding residues 1–444 (mature sequence numbering) that allowed us to produce an intact ectodomain (ggSC) containing domains D1-D4. Analysis of the resulting protein using size exclusion chromatography (SEC) with in-line multi-angle light scattering (MALS) revealed a molecular weight of 62.3kDa (Fig. 1B). This result is consistent with the predicted protein molecular weight of 50.3kDa plus ~12kDa of carbohydrates attached to four potential *N*-linked glycosylation sites, confirming that ggSC protein is monomeric and monodisperse.

Avian SC conformational flexibility

We previously reported a crystal structure and DEER spectroscopy analysis of hSC, which demonstrated that hSC adopts a compact triangular conformation stabilized by an interface between D1, D4 and D5 (15). Despite significant effort, we were unable to obtain well-ordered crystals of ggSC (data not shown). In the absence of a ggSC crystal structure, we sought to investigate its structure and conformational flexibility in solution using DEER spectroscopy, which measures the probability distribution of inter-nitroxide distances in a spin-labeled protein, thereby providing direct information that describes the structure and potential structural heterogeneity (18). Our strategy for ggSC involved monitoring spatial proximity between the first and last domains (D1 and D4). To accomplish this, we mutated two cysteine residues predicted to be surface exposed (Cys365 and Cys399) to alanine and introduced pairs of cysteine residues in ggSC D1 and D4 at residues Thr76, Glu352, and Ser387, sites homologous to those used previously to spin-label hSC (15) (Fig 2). The addition of nitroxide side chains (R1) at these sites resulted in ggSC variants D4-352R1/D4-387R1, D1-76R1/D4-352R1 and D1-76R1/D4-387R1. Labeled variants were monodisperse and indistinguishable from unlabeled protein as assayed by SEC (data not shown) and surface plasmon resonance (SPR) (Supplemental Fig. 1).

DEER time domain data and resulting distance distributions for D4-352R1/D4-387R1, which contained labels within D4, exhibited a single, narrow peak with a most probable distance of 32Å (Fig. 3A). These data are typical of measurements of R1 pairs in rigid protein structures (25), and the measured distance is comparable to the 25Å DEER measurement between homologous residues in hSC D5 (15).

In contrast, DEER time domain data and resulting distance distributions for D1-76R1/D4-352R1 and D1-76R1/D4-387R1, which monitor spatial proximity between D1 and D4, were multimodal and extended beyond experimental detection limits (~17–80Å), indicating that unliganded ggSC is flexible and that the distance between D1 and D4 is highly variable (Fig. 3B, 3C). This contrasts with results for hSC, in which analogous experiments revealed a narrow distribution and a single most-probable distance, indicating that D1 and D5 are always in contact (15). Although ggSC appears dynamic, it is notable that D1-76R1/

D4-352R1 and D1-76R1/D4-387R1 distance distributions exhibited defined peaks at ~20Å, 35Å, 55Å, and perhaps beyond the experiment detection limits, suggesting that ggSC exists in several defined states at equilibrium. The short-distance peaks at ~20Å and/or 35Å are comparable to distances measured between D1 and D5 in hSC (28Å between residues D1-67R1/D5-491R1), suggesting that ggSC can adopt a “closed” conformation in which D1 and D4 are in contact. However, long-distance peaks >35Å indicate that ggSC also exists in states in which D1 and D4 are separated. Thus in contrast to unliganded hSC, which is always closed (15), these results suggest that unliganded ggSC alternates between open and closed conformational states.

The observation that ggSC, which lacks a domain homologous to mammalian D2, exhibits increased conformational flexibility compared to hSC, motivated us to test D2 contributions to hSC dynamics. Accordingly, we engineered an hSC variant in which D2 was replaced with a linker equivalent to that linking avian D1 and D2, resulting in hSC D1-D3-D4-D5. We further modified this variant to mutate surface-exposed Cys468 and Cys502 to alanine and to introduce cysteine residues at positions Thr67 and Gln491 (full-length hSC sequence numbering). We labeled the resulting protein with the R1 nitroxide side chain to create an hSC D1-D3-D4-D5 D1-67R1/D5-491R1 variant. DEER time domain data and resulting distance distributions for this variant were broad, multimodal and extended beyond the detection limits of the experiment (Fig. 3D), similar to those for ggSC and in contrast to wild type hSC D1-67R1/D5491R1 (15) (Fig. 3D). Taken together, these results indicate that the mammalian D2 domain stabilizes unliganded SC in the closed conformation, and that in the absence of this domain (SC in birds, reptiles, and amphibians), the SC protein exhibits increased flexibility.

Avian SC-pIg Interactions

In addition to characterizing avian SC structure, we sought to investigate its ligand binding mechanism. Although avian pIg proteins are not readily available or well characterized, human pIg counterparts provide a reasonable substitution because they share sequence similarity (Supplemental Fig. 2) and the D1 domain from an amphibian SC homolog was previously shown to bind human pIgA (10).

We first tested the ability of intact ggSC to bind human dIgA. In mammals, a surface-exposed disulfide in D5 can form a covalent interaction with pIgA ligands (26) and because this disulfide is conserved in ggpIgR (residues Cys365 and Cys399; Fig. 2), we mutated these residues to alanine to prevent irreversible binding to ligand surfaces. Target proteins exhibited positive binding responses, however these responses did not fit a single-state binding model, and uncertainties in the binding mechanism prevented fitting the data with an accurate kinetic model. Nonetheless, qualitative differences in binding profiles were apparent. ggSC exhibited concentration-dependent binding characterized by a moderate association rate and slow dissociation rate, in which the protein only fully dissociated upon regeneration (Fig. 4A, 4D). Remarkably, ggSC dissociation from dIgA was slower than hSC dissociation from dIgA (15) (Fig. 4A, 4D, Supplemental Fig. 3A). These results suggested that avian SC binds human dIgA with higher affinity than it binds hSC, its cognate receptor. Because the mammalian SC D1 domain is well established to be both necessary and

sufficient for binding to pIg ligands (26), we engineered a ggD1-only variant, which also exhibited concentration-dependent binding to human dIgA (Fig. 4B, 4D). In this case, the binding profile was distinct from the binding of ggSC, exhibiting a rapid association and an initially rapid dissociation, which slowed and persisted throughout the experiment. Human D1 binding to dIgA was also reported to exhibit fast association and dissociation rates (15,27).

As noted above, mammalian SC can stabilize interactions with dIgA by forming a covalent bond between D5 and a cysteine residue on pIgA (26), but was also recently reported to use its D5 CDR1 and DE loops to mediate non-covalent interactions with dIgA (15). To determine if ggSC D4 CDR1 and DE loops also mediate non-covalent interactions with dIgA, we created a chimeric SC, ggSC tCDR1/tDE, in which the D4 CDR1 and DE loops were substituted with tSC counterparts having divergent sequences. An analogous human-fish SC chimera was previously reported to alter hSC-dIgA binding (15). While the ggSC tCDR1/tDE chimera exhibited concentration binding to dIgA, its binding profile was nearly indistinguishable from that of wild type ggSC (Fig. 4A, 4C, 4D). These observations suggest that the ggSC D4 CDR1 and DE loops do not play a detectable role in non-covalent interactions between ggSC D4 and dIgA, in contrast with results for hSC (15).

We also tested binding of the ggSC variants to human pIgM, observing concentration-dependent binding, in which ggSC exhibited moderate association and dissociation rates, ggD1 exhibited a moderate association and a slow dissociation, and ggSC tCDR1/tDE binding was indistinguishable from ggSC (Fig. 4E–H). Notably, the ggSC-pIgM binding profile exhibited a faster dissociation than that previously reported for hSC; however, ggD1 exhibited similar behavior to hD1 (15,27) (Fig. 4E, 4F, 4H, Supplemental Fig. 3C).

DISCUSSION

Here we report biochemical and structural characterization of an avian SC, which revealed shared and divergent characteristics when compared to mammalian counterparts. Differences between mammalian and avian SC can in part be attributed to the lack of a domain equivalent to mammalian D2 in birds (as well as in reptiles and amphibians). Our DEER data demonstrated that ggSC and the hSC D1-D3-D4-D5 variant both adopted heterogeneous solution structures with respect to the N-terminal (D1) and the C-terminal (D4 for ggSC or D5 for hSC) domains. The apparent structural heterogeneity of ggSC is consistent with our inability to grow well-ordered crystals.

While SC proteins lacking D2 adopt heterogeneous structures, peaks in the DEER probability distance distributions indicated that the heterogeneity arose from defined, rather than random, conformational states. Peaks in the 20–35Å range for both ggSC and hSC D1-D3-D4-D5 suggested that SC lacking D2 could adopt a closed conformation, in which the first and last domains are adjacent and form an interface. To explore this possibility, we created a model of a four-domain SC variant based on the hSC crystal structure (Fig. 5A). We found that removing D2 and modeling loop residues in geometrically-reasonable positions between D1 and D3 would theoretically allow the D1-D4-D5 and D3-D4 interfaces found in the hSC crystal structure to remain intact. However, because the positions of D1

and D3 were no longer stabilized by D2 and because the linkers between D1-D3 and D3-D4 were long and flexible, it is likely that D3 would occupy alternative positions even in a closed state.

Regardless of how a closed conformational state of ggSC might be stabilized, the DEER data indicated that it was in equilibrium with other states (long distance peaks), suggesting that in hSC, the addition of D2 stabilizes SC in a single (closed) state. A role for D2 in stabilizing the closed conformation was not anticipated because many of the residues found to stabilize the D1-D4-D5 interface in hSC are conserved or conservatively substituted in ggSC (Fig. 2), and D2 does not directly contact D4 or D5. However, D2 does contact D1 (and D3) and may serve to stabilize D1 in a position optimal for interface formation with D4-D5.

Peaks in ggSC and hSC D1-D3-D4-D5 DEER distance distributions occurring at longer range distances also suggested that alternative states, in which the first and last domains are separated, dominated conformational space. The defined states observed as peaks near 55Å and beyond could be related to ligand-binding intermediate states because hSC undergoes massive conformational changes that result in similar distance distributions when bound to dIgA and pIgM ligands (15). Thus, unliganded avian SC might exist in equilibrium between closed, ligand-bound, and/or binding intermediate conformations. Because our DEER experiments cannot measure distances beyond ~70Å, we cannot calculate a full distance distribution, accurately gauge the amount of time the protein spends in each state, or determine all possible states (e.g. states in which D1 and D4 are separated by more than 70Å).

Our binding experiments demonstrated that mechanisms of pIgR ligand binding are partially conserved from birds to mammals. This is further supported by the data demonstrating that ggSC D1 is necessary and sufficient for ligand binding to both pIgA and pIgM. These results are consistent with conservation at sites implicated in ligand binding such as D1 CDR1 (Fig. 2), and previously-reported binding between amphibian D1 and human pIgA (10). Although avian SC is more conformationally dynamic than hSC, and its shorter length might be expected to constrain its ability to bind ligand, our experiments indicated that avian D2-D3-D4 (mammalian D3-D4-D5) also contributed to binding because binding profiles of ggSC and ggD1 were different (Fig. 4A, 4B, 4D, 4E, 4F, 4H). By analogy, D2-D5 in hSC have been similarly reported to contribute to binding (15).

Despite these similarities, differences between ggSC and hSC binding to human dIgA were apparent. For example, ggSC binding profiles, characterized by a slow dissociation, were distinct from those of hSC and from hSC D1-D3-D4-D5 (Fig. 4A, 4D, Supplemental Fig. 3A, 3B) (15). In fact, comparison of binding of the two SC proteins lacking D2 (ggSC and hSC D1-D3-D4-D5; orange and grey dashed lines in Fig. 4D), revealed marked differences in binding profiles and likely, affinities. These observations suggest that differences between avian SC and hSC extend beyond the presence or absence of the D2 domain. Furthermore, we found that the binding of human dIgA by chimeric ggSC tCDR1/tDE and ggSC were similar (Fig. 4A, 4C, 4D), suggesting that the CDR1 and DE loops did not contribute to ligand binding by ggSC to the same extent as reported for equivalent motifs in hSC (15).

The ability of pIgR to bind and transport pIgM in lower vertebrates is assumed, but to the best of our knowledge, has not been demonstrated directly. Previous work showed that chimeric pIgR expressing Xenopus D1 and human D2-D5 could bind human pIgA but not pIgM (10), and among mammals, the extent to which pIgR transports pIgM varies with species (28). Binding has been postulated to depend on the identity of the residue at the center of the D1 CDR2 loop (Glu53 in hSC) (27,28). Given these observations, our ability to detect binding between ggSC and human pIgM is notable, especially because the residue at the center of the ggSC D1 CDR2 loop is a serine (Fig. 2). While our experiments detected ggSC binding to human pIgM, it remains unclear if avian pIgR actively transports pIgM *in vivo*. Nonetheless, demonstration of interactions between non-cognate SC and pIg proteins indicate that the mechanisms of pIgR binding to pIgM and pIgA are at least in part conserved despite significant evolutionary changes in both pIgR and pIg ligands.

Perhaps the most notable finding of this work is that with the transition from birds to mammals, unliganded pIgR/SC has evolved to exist in different conformations. Together with previous studies of fish and mammalian SC (15), our results support a model in which SC first existed as a two-domain, elongated molecule (fish) and subsequently evolved into a four-domain molecule capable of adopting a range of conformations (birds; likely also amphibians and reptiles) (Fig. 5B). Ultimately, SC evolved into a five-domain variant that adopts a compact conformation, yet maintains an ability to change conformation upon ligand binding. These observations support the possibility that the addition of D2 and the evolution of the associated closed conformation conferred functional advantages in mammals that are likely to include, but may extend beyond, a role in ligand binding. The closed state may enhance unliganded SC's innate immune function to bind bacteria (15), and the addition of D2 may have provided mammals with an advantage parallel to physiological changes in mucosal tissues. For example, mammals differ from birds in that mammary glands produce breast milk that is rich in SC (and secretory IgA, the complex of SC and pIgA) and is important for the establishment of infant intestinal microbiota. Additionally, mammals and birds likely have divergent relationships with mucosal microbiota, for which different molecular liaisons may be advantageous. Regardless of which selective pressures have shaped SC and its pIg ligands, the structural and mechanistic differences we characterized among SCs from divergent vertebrates support the hypothesis that mucosal immune function has been finely tuned throughout vertebrate evolution.

Supplementary Material

Refer to Web version on PubMed Central for supplementary material.

Acknowledgments

This work was funded by: This work was funded by: National Institute of Allergy and Infectious Diseases AI04123 to PJB, The Cancer Research Institute Irving Postdoctoral Fellowship to BMS, The Jules Stein Professorship Endowment to WLH, and National Institutes of Health EY005216 to WLH.

We thank Jost Vielmetter and the Caltech Protein Expression Center for assistance with protein expression. We also thank members of the Bjorkman and Hubbell labs for insightful discussions.

References

1. Kaetzel CS. Coevolution of Mucosal Immunoglobulins and the Polymeric Immunoglobulin Receptor: Evidence That the Commensal Microbiota Provided the Driving Force. ISRN Immunology. 2014; 2014:20.
2. Mostov KE, Kraehenbuhl JP, Blobel G. Receptor-mediated transcellular transport of immunoglobulin: synthesis of secretory component as multiple and larger transmembrane forms. Proc Natl Acad Sci U S A. 1980; 77:7257–7261. [PubMed: 6938972]
3. Kaetzel CS. The polymeric immunoglobulin receptor: bridging innate and adaptive immune responses at mucosal surfaces. Immunol Rev. 2005; 206:83–99. [PubMed: 16048543]
4. Lindh E. Increased risistance of immunoglobulin A dimers to proteolytic degradation after binding of secretory component. J Immunol. 1975; 114:284–286. [PubMed: 1090649]
5. Akula S, Mohammadamin S, Hellman L. Fc receptors for immunoglobulins and their appearance during vertebrate evolution. PLoS One. 2014; 9:e96903. [PubMed: 24816777]
6. Mostov KE, Friedlander M, Blobel G. The receptor for transepithelial transport of IgA and IgM contains multiple immunoglobulin-like domains. Nature. 1984; 308:37–43. [PubMed: 6322002]
7. Flajnik MF. All GOD's creatures got dedicated mucosal immunity. Nat Immunol. 2010; 11:777–779. [PubMed: 20720582]
8. Hamuro K, Suetake H, Saha NR, Kikuchi K, Suzuki Y. A teleost polymeric Ig receptor exhibiting two Ig-like domains transports tetrameric IgM into the skin. J Immunol. 2007; 178:5682–5689. [PubMed: 17442951]
9. Sunyer JO. Fishing for mammalian paradigms in the teleost immune system. Nat Immunol. 2013; 14:320–326. [PubMed: 23507645]
10. Braathen R, Hohman VS, Brandtzaeg P, Johansen FE. Secretory antibody formation: conserved binding interactions between J chain and polymeric Ig receptor from humans and amphibians. J Immunol. 2007; 178:1589–1597. [PubMed: 17237408]
11. Magadan-Mompo S, Sanchez-Espinel C, Gambon-Deza F. IgH loci of American alligator and saltwater crocodile shed light on IgA evolution. Immunogenetics. 2013; 65:531–541. [PubMed: 23558556]
12. Wieland WH, Orzaez D, Lammers A, Parmentier HK, Verstegen MW, Schots A. A functional polymeric immunoglobulin receptor in chicken (Gallus gallus) indicates ancient role of secretory IgA in mucosal immunity. Biochem J. 2004; 380:669–676. [PubMed: 14992684]
13. Feng LN, Lu DQ, Bei JX, Chen JL, Liu Y, Zhang Y, Liu XC, Meng ZN, Wang L, Lin HR. Molecular cloning and functional analysis of polymeric immunoglobulin receptor gene in orange-spotted grouper (Epinephelus coioides). Comp Biochem Physiol B Biochem Mol Biol. 2009; 154:282–289. [PubMed: 19602447]
14. Rombout JH, van der Tuin SJ, Yang G, Schopman N, Mroczek A, Hermsen T, Taverne-Thiele JJ. Expression of the polymeric Immunoglobulin Receptor (pIgR) in mucosal tissues of common carp (Cyprinus carpio L.). Fish & shellfish immunology. 2008; 24:620–628. [PubMed: 18356080]
15. Stadtmueller BM, Huey-Tubman KE, Lopez CJ, Yang Z, Hubbell WL, Bjorkman PJ. The structure and dynamics of secretory component and its interactions with polymeric immunoglobulins. eLife. 2016; 5
16. Tarazona MP, Saiz E. Combination of SEC/MALS experimental procedures and theoretical analysis for studying the solution properties of macromolecules. Journal of biochemical and biophysical methods. 2003; 56:95–116. [PubMed: 12834971]
17. Jeschke G, Polyhach Y. Distance measurements on spin-labelled biomacromolecules by pulsed electron paramagnetic resonance. Physical chemistry chemical physics : PCCP. 2007; 9:1895–1910. [PubMed: 17431518]
18. Jeschke G. DEER distance measurements on proteins. Annual review of physical chemistry. 2012; 63:419–446.
19. Sievers F, Wilm A, Dineen D, Gibson TJ, Karplus K, Li W, Lopez R, McWilliam H, Remmert M, Soding J, Thompson JD, Higgins DG. Fast, scalable generation of high-quality protein multiple sequence alignments using Clustal Omega. Molecular systems biology. 2011; 7:539. [PubMed: 21988835]

20. Robert X, Gouet P. Deciphering key features in protein structures with the new ENDscript server. Nucleic acids research. 2014; 42:W320–324. [PubMed: 24753421]
21. Gouet P, Courcelle E, Stuart DI, Metoz F. ESPript: analysis of multiple sequence alignments in PostScript. Bioinformatics. 1999; 15:305–308. [PubMed: 10320398]
22. Gouet P, Robert X, Courcelle E. ESPript/ENDscript: Extracting and rendering sequence and 3D information from atomic structures of proteins. Nucleic acids research. 2003; 31:3320–3323. [PubMed: 12824317]
23. Emsley P, Cowtan K. Coot: model-building tools for molecular graphics. Acta Crystallogr D Biol Crystallogr. 2004; 60:2126–2132. [PubMed: 15572765]
24. Peppard JV, Rose ME, Hesketh P. A functional homologue of mammalian secretory component exists in chickens. Eur J Immunol. 1983; 13:566–570. [PubMed: 6409654]
25. Lerch MT, Yang Z, Brooks EK, Hubbell WL. Mapping protein conformational heterogeneity under pressure with site-directed spin labeling and double electron-electron resonance. Proc Natl Acad Sci U S A. 2014; 111:E1201–1210. [PubMed: 24707053]
26. Hamburger AE, Bjorkman PJ, Herr AB. Structural insights into antibody-mediated mucosal immunity. Curr Top Microbiol Immunol. 2006; 308:173–204. [PubMed: 16922091]
27. Hamburger AE, West AP Jr, Bjorkman PJ. Crystal structure of a polymeric immunoglobulin binding fragment of the human polymeric immunoglobulin receptor. Structure. 2004; 12:1925–1935. [PubMed: 15530357]
28. Roe M, Norderhaug IN, Brandtzaeg P, Johansen FE. Fine specificity of ligand-binding domain 1 in the polymeric Ig receptor: importance of the CDR2-containing region for IgM interaction. J Immunol. 1999; 162:6046–6052. [PubMed: 10229845]

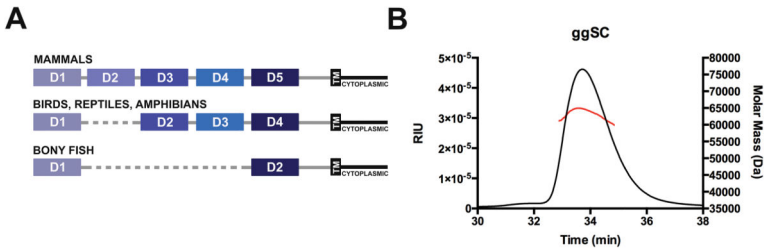

Figure 1. pIgR domain organization and SEC-MALS data

(A) Schematic showing the domain organization of the pIgR protein from humans, birds, reptiles, amphibians, and teleost fish. Each mammalian domain (D1-D5) is indicated by color and domains from other species are colored according to their mammalian homolog. (B) SEC-MALS data for ggSC showing elution time versus refractive index units (RIU) and Molar Mass (Da).

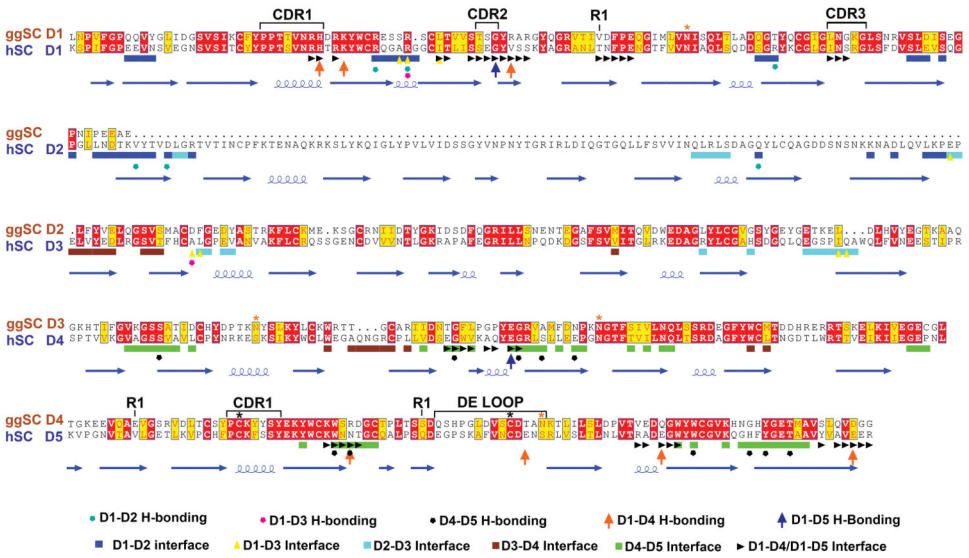

Figure 2. Comparison of ggSC and hSC sequences

Sequence alignment of ggSC (top) and hSC (bottom) with domain numbering for ggSC (orange) and hSC (blue) indicated. The locations of regions implicated in mammalian SC-pIg interactions, including D1 CDR loops and D5 CDR1 and DE loops, are indicated above the ggSC sequence along with the position of Cys residues involved in potential covalent binding to pIgA (black asterisk), ggSC potential *N*-linked glycosylation sites (orange asterisk), and residues mutated to Cys for nitroxide labeling (R1). The hSC secondary structure elements, determined from the hSC crystal structure (15), are shown below the hSC sequence along with residues found to stabilize domain interfaces (colored according to the key below the sequence alignment).

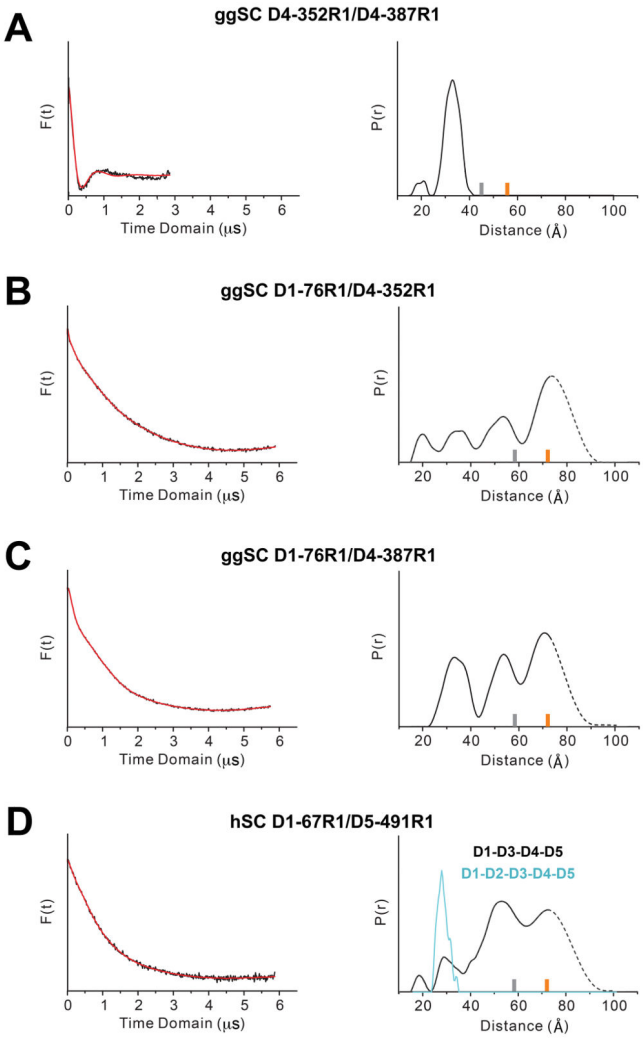

Figure 3. DEER data

(A–D) Time domain data (left) and associated distance distribution, probability [P(r)] versus distance (Å), for the indicated mutants obtained after model-free fitting of the dipolar evolution function (right). The gray and orange bars indicate the upper limit of reliable distance and shape of the distribution (see Materials and Methods). Distances 70 Å are beyond detection limits (dashed traces).

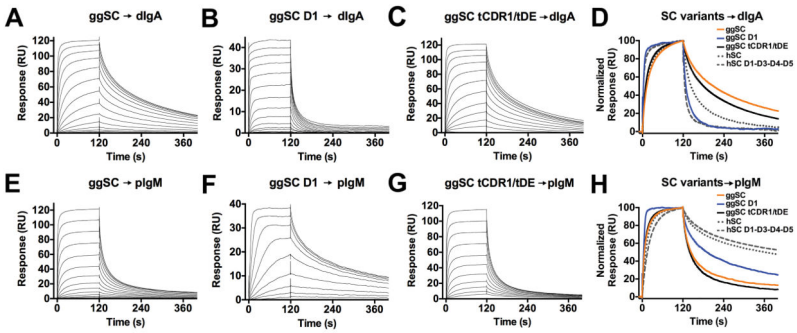

Figure 4. ggSC and hSC binding to dIgA and pIgM

(A–C) Sensorgrams showing ggSC, ggSC D1, ggSC tCDR1/tDE binding human dIgA. The highest concentration for all variants binding to human dIgA was 1024nM. (D) Overlay of the normalized binding response for concentration-matched samples (32nM) from A–C and Supplemental Fig. 3A, 3B, (hSC and hSC D1-D3-D4-D5). (E–G) Sensorgrams showing ggSC, ggSC D1, ggSC tCDR1/tDE binding human pIgM. Highest concentrations of ggSC variant binding to human pIgM were: 32nM (ggD1), 1024nM (ggSC), 1024nM (ggSC tCDR1/tDE). (H) Overlay of the normalized binding response for concentration-matched samples (32nM) from E–G and Supplemental Fig. 3C, 3D, (hSC and hSC D1-D3-D4-D5). Sensorgrams shown are equivalent to those obtained from replicate, independent experiments (not shown).

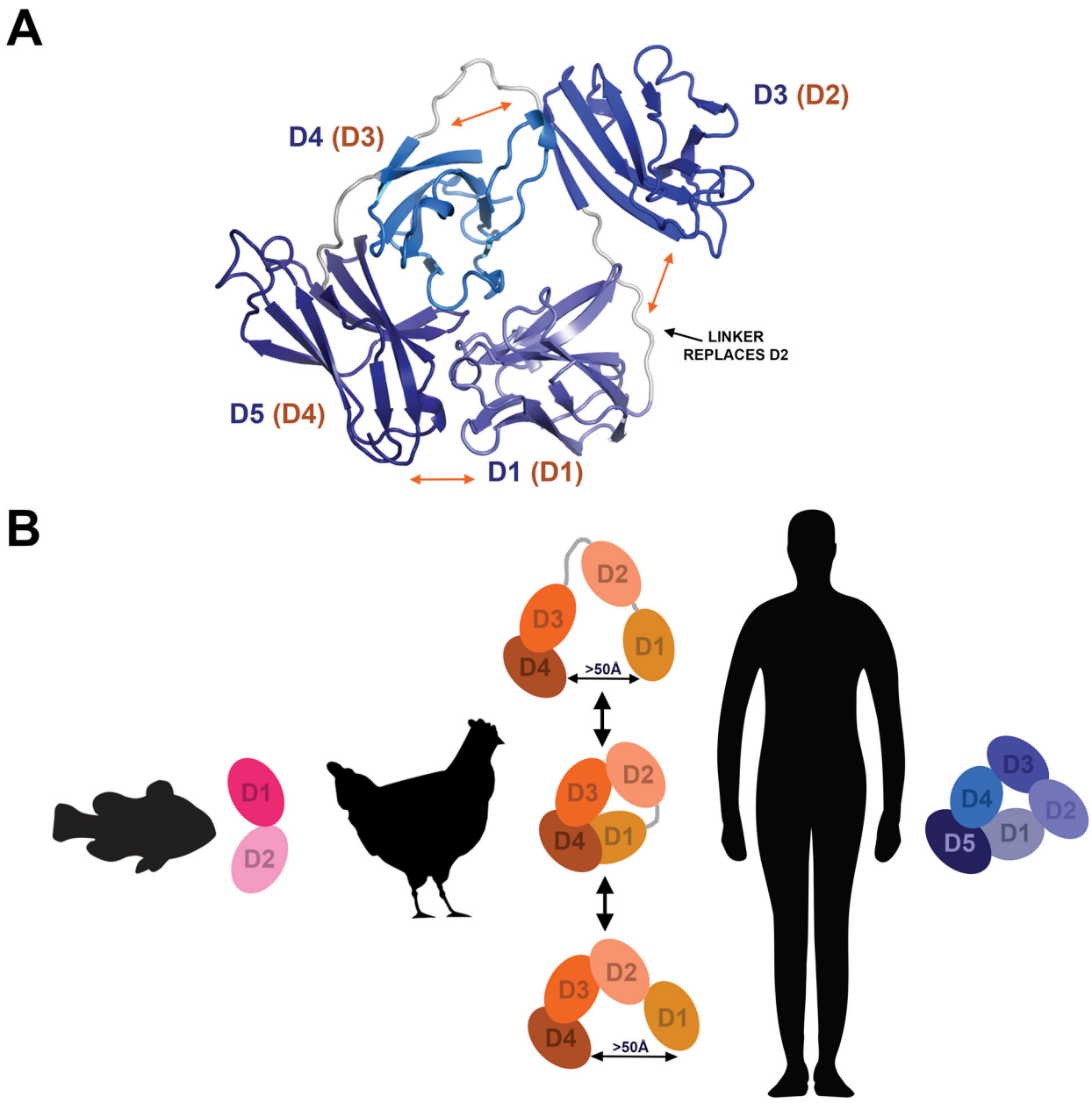

Figure 5. Models of SC variants

(A) Model of a closed four-domain SC variant based on the hSC crystal structure with loop residues (which replace D2; black arrow) modeled in geometrically reasonable positions. Labels indicate mammalian SC domain identity (blue) and avian SC domain identity (orange, parentheses) and orange arrows indicate putative regions of flexibility. (B) Schematic summary of SC conformation throughout evolution. Fish SC has just two domains and exists in an open conformation; avian SC has four domains and exists in an equilibrium between open and closed states; hSC remains closed until encountering ligand.